Improved Icephobic Properties on Surfaces with a Hydrophilic Lubricating Liquid

Salih Ozbay, Cigdem Yuceel, and H. Yildirim Erbil*

Department of Chemical Engineering, Gebze Technical University, Gebze 41400, Kocaeli, Turkey

S *Supporting Information*

ABSTRACT: Slippery liquid-infused porous surfaces were developed recently for icephobic surface applications. Perfluorinated liquids, silicone oil, hydrocarbon, and water were used as lubricating liquids to form a continuous layer on a suitable substrate to prevent icing. However, ice accretion performances of these surfaces have not been reported previously depending on the type of the lubricant. In this work, fluorinated aliphatics, polyalphaolefin, silicone oil, and decamethylcyclopenta siloxane were used as hydrophobic lubricants; water, ethylene glycol, formamide, and water−glycerine mixture were used as hydrophilic lubricants to be impregnated by hydrophobic polypropylene and hydrophilic cellulose-based filter paper surfaces; ice accretion, drop freezing delay time, and ice adhesion strength properties of these surfaces were examined; and the results were compared to those of the reference surfaces such as aluminum, copper, polypropylene, and polytetrafluoroethylene. An ice accretion test method was also developed to investigate the increase of the mass of formed ice gravimetrically by spraying supercooled water onto these surfaces at different subzero temperatures ranging between −1 and −5 °C. It was determined that hydrophilic solvents (especially a water−glycerine mixture) that impregnated hydrophilic porous surfaces would be a promising candidate for anti-icing applications at −2 °C and 56−83% relative humidity because ice accretion and ice adhesion strength properties of these surface decreased simultaneously in these conditions.

KEYWORDS: *icephobic, anti-icing, ice accretion, ice adhesion, drop freezing time, SLIPS, contact angle*
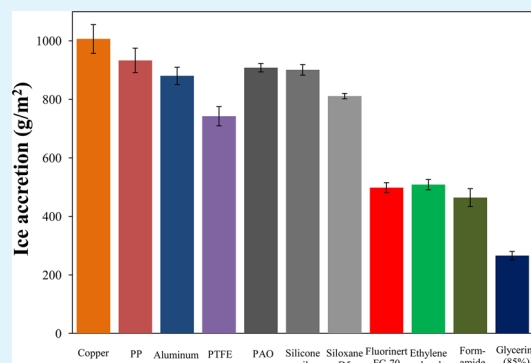
INTRODUCTION

Ice or snow accumulation on surfaces causes improper working or breakdown of many critical systems such as aircraft,[1] wind turbines,[2−4] power lines,[5] offshore platforms,[6] photovoltaic devices,[7] cars, trains, and ships, which results in large economic damage and loss of lives. Ice removal methods can be classified into two categories: active and passive. Active solutions are currently widely used including mechanical scraping, thermal treatments, and applying deicing fluids to remove ice after it has been deposited; however, these methods are usually expensive due to the high energy requirements. Passive solutions include the formation of icephobic or anti-icing surfaces that would prevent the ice from adhering onto them or from being easily delaminated afterward by natural airflows or solar radiation. Intensive efforts have been made to develop suitable anti-icing surfaces and to understand the mechanism of ice formation and surface icephobicity, and many extensive reviews were published on this subject in the past decade.[3−5,7,9−12] Unfortunately, passive methods have found very few industrial applications because of their limited success in ice repellency, and currently there is no known material that can completely prevent ice or snow from accumulating on a surface.[7,9,10]

Superhydrophobic surfaces[13,14] that exhibit a water contact angle greater than 150° where water droplets roll of readily from the surface at a small tilt angle were applied as anti-icing coatings in recent years.[15−36] Many researchers hypothesized that artificial superhydrophobic surfaces that were prepared by the combination of low surface energy materials and enhanced surface roughness would have been successful in the anti-icing field by repelling the water droplets and eliminating their presence on a surface before they can freeze.[15−27] In contrast, many researchers reported that the use of superhydrophobic surfaces was not successful for anti-icing applications.[7,8,10,28−36] It was shown that superhydrophobicity is lost especially in high humidity conditions or can be destroyed under the deicing process, and ice adhesion strength would be enlarged when ice penetrates into their surface texture. Moisture condenses in the rough structure of a superhydrophobic surface over time under high humidity conditions, and droplets will grow and coalescence rapidly to form an ice layer on the surface. Varanasi and co-workers[28] reported that frost nucleation occurs on all areas of the superhydrophobic surface textures, leading to the loss of superhydrophobic properties and ice adhesion strength increases. Kulinich and co-workers[30,32] have shown that when ice accretion eventually occurs on a superhydrophobic surface, it causes gradual damage of the surface

microstructure during icing and deicing. In addition, ice adhesion strength on these surfaces is significantly higher in a humid atmosphere. Chen et al.[33] have also reported that superhydrophobic surfaces cannot reduce ice adhesion, and ice adhesion strength on flat hydrophilic and hydrophobic surfaces was lower than structured superhydrophilic and super-hydrophobic surfaces. Nosonovsky and Hejazi[34] presented an analysis on why superhydrophobic surfaces are not always icephobic. They stated that the force needed to detach ice pieces from a surface depends on the receding contact angle and also on the initial size of interfacial cracks, and even surfaces with a very high receding contact angle may have strong adhesion to ice if the size of the cracks is small.[34] In conclusion, the use of superhydrophobic surfaces for anti-icing applications is under question, and new routes for this practical problem are needed.

On the other hand, the wettability of a surface was proposed to be an important parameter in choosing the type of coating material to resist icing or snow formation on a surface.[16,31,37−42] However, there are conflicting reports on this matter in the literature. For example, Saito et al.[37] showed low ice adhesion performance of polytetrafluoroethylene containing superhydro-phobic surfaces. Meuler et al.[38] found a relationship between the equilibrium and receding contact angles of water and ice adhesion strength. Kulinich and Farzaneh reported that ice adhesion strength decreased with the decrease of the contact angle hysteresis of the surface.[16] Yin et al.[39] prepared representative superhydrophilic, hydrophilic, hydrophobic, and superhydrophobic surface samples and applied ice accretion tests by spraying supercooled water on samples at different horizontal inclination angles, and a correlation between surface wettability and ice formation was not observed in this work.[40] Yang et al.[40] tested fluoropolymer surfaces in anti-icing applications, and their results show that polymers having a smooth surface can significantly reduce ice adhesion strength but do not show an obvious effect in reducing ice accretion at −8 °C. Some researchers proposed that the use of hydrophilic surfaces resulted in better freezing delay properties.[31,41] Poulikakos and co-workers[10,31] reported that hydrophilic surfaces with nanometer-scale roughness showed unexpectedly long freezing delays, at least 1 order of magnitude longer than typical superhydrophobic surfaces with larger roughness and low wettability. Li et al.[42] found that the normalized surface ice nucleation rate on a flat hydrophilic surface is about 1 order of magnitude lower than that on a flat hydrophobic surface by applying evaporation, condensation, and subsequent ice formation process in a closed cell. Unfortunately, the effect of the wettability of a surface on its icephobicity properties is a very complex phenomenon and was not well understood.

Recently, a novel idea to obtain icephobic surfaces was introduced via biomimetics: Aizenberg and co-workers[43−48] developed a slippery liquid-infused porous surface (SLIPS) inspired by Nepenthes pitcher plants to be used for anti-icing applications. A film of perfluorinated lubricating liquid was infused to form a continuous liquid lubricating layer on a porous polymeric substrate such as low-surface-energy structured Teflon and epoxy resin. The lubricant hemiwicks into the texture and spreads across the tops of the surface texture features. When water droplets were deposited on this porous SLIPS layer, a composite solid−lubricant−water interface forms, and the droplet slides easily at a small tilt angle. A "SLIPS" layer effectively repels complex fluids, such as crude oil, and also repels ice even in a high humidity

environment (e.g., 60% relative humidity) by removing the condensed water.[43] The same group then prepared SLIPS-coated aluminum surfaces by using electrochemically coated nanostructured polypyrrole on aluminum sheet and hydro-phobized by a fluorosilane and then covered by applying droplets of a perfluorinated lubricant and reported that SLIPS-coated aluminum surfaces not only significantly reduce ice accumulation by allowing the condensed water droplets to slide off before they freeze but also enable the easy removal of the accumulated ice and melted water by gravity at low tilt angles.[44]

The mechanism of the icephobicity of the SLIPS was explained as follows: ice formation happens via two routes, impact of supercooled water droplets on surfaces at subzero temperatures and direct ice condensation from the vapor phase of a super saturated humid ambient. Contact angle hysteresis is the difference of advancing and receding contact angles and is generally a measurement of the surface roughness and chemical heterogeneity of a surface.[49,50] The three-phase contact line of a droplet pins at surface defects, and the smaller is the contact angle hysteresis, the smaller is the force tangent to the surface that is needed to move the drop. Thus, both the magnitude of contact surface area and the ease of sliding drops on a surface are important parameters to affect icephobicity. If the infused liquid has a freezing point well below the temperature to be used in anti-icing applications, then this SLIPS minimizes contact angle hysteresis because the interface between infused liquid and water minimizes the contact line pinning and would impart icephobicity.[43,45] The invention of SLIPS led to many similar publications in the anti-icing field after 2012.[51−65] Two recent reviews on the synthesis and properties of SLIPS were also published.[9,10]

However, the main weakness of a SLIPS is its durability, which is limited by how long the perfluorinated lubricant stays in the pores without evaporating or leaking. Another important problem is the high cost of the perfluorinated liquid lubricants used in SLIPS. Varanasi and co-workers[51−54] showed that there was another trouble: the lubricant may spread over and "cloak" the water droplets that would form on the lubricant-impregnated surfaces (LIS). This is important because cloaking can cause the progressive loss of impregnated lubricating oil through entrainment in the water droplets as they are shed from the surface.[51] Condensed water droplets on the perfluoroether lubricant impregnated surfaces cannot be evaporated even under high superheat conditions, suggesting that cloaking occurred during condensation. These water or ice droplets will be pinned to the texture probably at the post tops, and the longevity of a LIS surface is affected by lubricant cloaking, drainage, and miscibility.[51] In another publication, they pointed out that the anti-icing results of LIS are promising if the surfaces used in the studies had thick excess lubricant films atop the textured solid, but such excess films are unstable and will drain to attain thermodynamically stable configurations in the presence of external forces such as gravity and drag forces.[52] The ice adhesion strength on LIS in a stable thermodynamic state is higher than that with the excess lubricant layer, and the ice adhesion strength on LIS's with a thermodynamically stable lubricant layer is texture-dependent and decreases with increasing texture density.[53] Varanasi and co-workers also studied frost formation on nanostructured and microstructured superhydrophobic surfaces with and without the perfluorinated oil layer.[54] They observed that any LIS with perfluorinated oil was susceptible to irreversible damage, which was caused by oil migration from the wetting ridge by capillary

attraction onto frozen drops, and the anti-icing and self-healing characteristics of the surface are lost within a few frosting and defrosting cycles. Hence, the use of liquid reservoirs that allows the replenishment of the lubricant would become necessary for the sustained performance of LIS. The authors proposed that further research is necessary to develop liquid-texture pairs, which will significantly decrease the rate of oil depletion into frost.[54] Later, Aizenberg's group[48] reported that the thermodynamical stability of SLIPS could be improved by employing a closed-cell architecture using an inverse colloidal monolayer template to design transparent, nanoporous SLIPS structures. The lubricants could be firmly locked in the structures, and the lubricant-infused layers demonstrated good thermodynamical stability of over 9 months vertical storage with very low ice adhesion strength on this surface.[48]

Meanwhile, inspired by ice skating, Jiang, Wang, and co-workers fabricated SLIPS with a self-lubricating liquid water layer for anti-icing applications.[55−58] They grafted cross-linked hygroscopic poly(acrylic acid) inside the micropores of patterned silicon wafer surfaces. This hygroscopic polymer network swells and liquefies due to water absorption or condensation and thus bulges out of micropores, enabling the merging of the swollen polymers to form a self-lubricating liquid water layer.[55] Ice adhesion on this surface is 1 order of magnitude lower than that on the superhydrophobic surfaces. It is possible that a self-lubricating liquid water layer can form whenever ice or frost is placed atop of the coating by melting in both low and high humidity environments.[55] In another work, they fabricated organogel-based easy-sliding surfaces through free radical copolymerization of butyl methacrylate and lauryl methacrylate monomers on various substrates, including silicon wafer, microstructured silicon posts, aluminum, copper, and iron.[56] The organogel was swollen with low viscosity silicon oil. The authors reported that the easy-sliding property of these organogel-modified surfaces can provide superior self-cleaning; however, no anti-icing tests were carried out.[56] Recently, the same group used polyurethane as the main component for a new durable anti-icing coating with an aqueous lubricating layer.[57] Polymers with hydrophilic pendant groups were synthesized; the introduced hydrophilic component can absorb water in humid environments, forming a lubricating water layer on the surface even at subzero environments. The ice adhesion strengths of this polyurethane coating with an aqueous lubricating layer were reduced substantially on metals, metal alloys, ceramics, and polymer surfaces. The formed ice on this anti-icing coating can be blown off by wind action in a wind tunnel. Unfortunately, no ice accretion experiments were reported for this coating.[57] Hyaluronic acid and dopamine were also used in the anti-ice coating to form aqueous lubricating layer.[58] Chen et al.[59] synthesized transparent slippery surfaces made with porous cellulose lauroyl ester films using perfluoropolyether lubricant, which delays ice formation.

Instead of perfluorinated oil or water lubricant, other liquids such as silicone oils were also applied as lubricant on SLIPS.[60,61] Zhu et al.[60] prepared silicon-oil-infused polydimethylsiloxane (PDMS) coatings for icephobic applications. The authors reported that when 20−40 wt % silicon oil is impregnated, the ice adhesion tensile strength is only about 5% on bare aluminum surface. It was shown that, although high amounts of loose ice were formed on a silicone oil containing PDMS surface, this type of ice can be easily removed from the surface, even by natural forces such as vibration, wind, and

gravity.[60] In another work,[61] no PDMS was used, but instead a substrate is covered with a thin silicone-oil film annealed for 2−3 min at 300 °C. Heating of the substrate leads to the formation of a thin silicone layer on the surface, after which it is impregnated with silicone oil giving a water-repellent surface with very low contact angle hysteresis. An icephobic strategy is also developed by combining PDMS containing SLIPS and photothermal effect to delay ice accumulation and to remove ice easily.[62] An electrospray method coupled with phase separation was also applied to prepare heptadecafluorodecyl trimethoxysilane fluorinated hierarchically microstructured high temperature vulcanized silicone rubber substrates infiltrated with a perfluoropolyether lubricant to form the SLIPS, and long delay time for ice formation and low ice adhesion results are reported on these surfaces.[63] An organogel anti-icing coating is created by swelling cross-linked polydimethylsiloxane networks with liquid paraffin where polymer network absorbs and holds the paraffin to avoid being removed during the shed off of the accreted ice, and this coating was found to exhibit ultralow ice adhesion strength.[64] Self-lubricating transparent organogels are also prepared via a cross-linking reaction of polydimethylsiloxanes in the presence of several organic liquids such as aliphatic and aromatic hydrocarbons, silanes, and siloxanes. A liquid layer is continuously formed on the topmost of these surfaces under appropriate conditions due to the syneresis of organogels showing anti-icing properties.[65]

It is stated that further research is necessary to develop impregnated lubricant and supporting solid pairs, to significantly increase icephobicity of the lubricant infused surfaces.[7,10] However, a question still persists, of what would be the type of the lubricant; would it be hydrophilic or hydrophobic? Most of the researchers used hydrophobic lubricating liquids such as perfluorinated oils,[43−48] silicone oils,[60−65] or hydrocarbons,[65] and few used hydrophilic ones such as water.[55−58] Another unanswered question is the type of the solid supporting texture; would it be hydrophilic or hydrophobic? To the best of our knowledge, there is no paper focusing on these important questions.

In this study, we searched the answers of the above questions and prepared hydrophobic fluorinated aliphatics (Fluorinert FC-70), polyalphaolefin (PAO), silicone oil (SiO), decamethylcyclopenta siloxane (Siloxane D5), and hydrophilic ethylene glycol (EG), formamide (FA), water, and water−glycerine mixture containing 85% glycerine by weight (GLY-85%) impregnated hydrophobic polypropylene (PP) and hydrophilic cellulose-based filter paper (FP) surfaces, we examined the ice accretion quantity and freezing delay time and ice adhesion strength properties of these surfaces, and we compared the results with four reference materials, aluminum, copper, polypropylene, and polytetrafluoroethylene (PTFE) surfaces. A suitable ice accretion test method was also developed to investigate the increase of the mass of formed ice on the test surfaces gravimetrically by spraying supercooled water onto these surfaces at different subzero temperatures ranging between −1 and −5 °C. It was found that the ice accretion on the hydrophilic EG, FA, and especially GLY-85% impregnated surfaces was substantially lower than that on other solvent impregnated surfaces and the solid reference surfaces. In addition, hydrophilic filter paper support performed better with these hydrophilic liquids than hydrophobic supports, and the reasons are discussed.
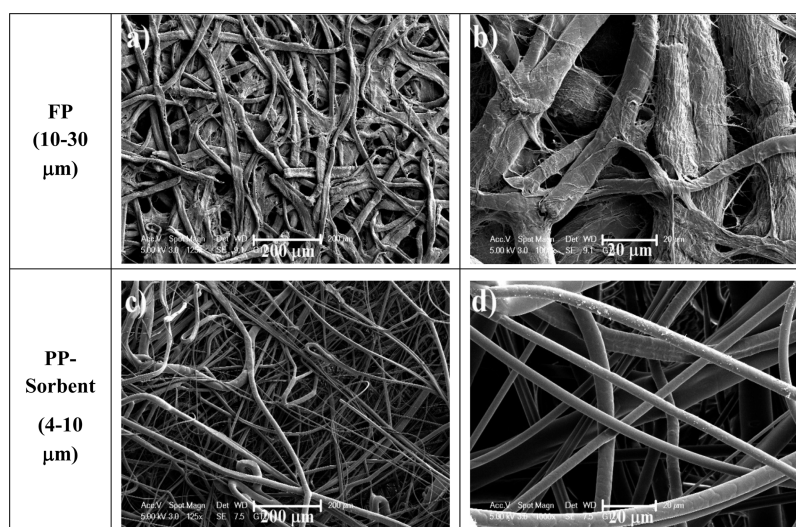
Figure 1. SEM images of filter paper (FP) and polypropylene (PP)-sorbent sheet before solvent impregnation: (a) FP surface with 125× magnification; (b) FP surface with 1000× magnification; (c) PP-sorbent surface with 125× magnification; and (d) PP-sorbent surface with 1000× magnification.

■ EXPERIMENTAL SECTION

Materials. Commercial sheets of aluminum (Al), copper (Cu), PP, and PTFE supplied in Turkey were used for experiments. Al, PP, and PTFE sheets were cut in 76 mm × 78 mm size and cleaned with acetone, ethyl alcohol, and deionized water consecutively and dried in an oven before use. Cu sheets having the same size were cleaned with dilute hydrochloric acid and rinsed with deionized water and dried. Polyalphaolefin-6 (PAO-6) was kindly supplied from Dolunay Madeni Yaglar, Turkey. Silicone oil (350 cSt) was purchased from Epsilon Kimya, Turkey. Glycerine was purchased from BDH Chemicals. Decamethylcyclopenta siloxane (Siloxane D5), ultrapure water, ethylene glycol, and formamide were purchased from Merck. Fluorinert FC-70 (a mixture of completely fluorinated aliphatic compounds) was purchased from Alfa Aesar. PP sorbent sheets in white color made of polypropylene fibers that are bonded together creating a surface for high absorption speed were kindly supplied from Mavideniz Cevre Hizmetleri A.S., Turkey. PP sorbent sheets are mostly used to adsorb oils and other materials in industry and also to clean petroleum spills on the sea. Schleicher and Schuell (ref no: 300011) ashless black ribbon filter paper (FP) was used in our experiments. The circular sheet samples of FP and PP were cut having a diameter of 85 mm. Fiber diameters of FP range between 10 and 30 μm and are 3−4 times larger than that of the PP-sorbent sheet (4−10 μm) as seen in the SEM images of blank FP and PP-sorbent sheets (before solvent impregnation) in Figure 1.

Solvent Impregnation. SiO, PAO, Siloxane D5, and Fluoroinert FC-70 were used as hydrophobic solvents; EG, FA, and 15% water−85% glycerine by weight mixture (GLY-85%) were used as hydrophilic solvents. Glycerine was diluted with pure water to 85% concentration to decrease the freezing point of pure glycerine from +17.8 to −10.9 °C and also to lower its solution viscosity for the ease of solvent impregnation into substrates. PP-sorbent sheet and FP were placed in these solvents for 1 h to reach the maximum weight increase and then hung vertically for 15 min to drain the excess solvent to prepare the solvent impregnated surfaces before testing.

Ice Accretion Test. Ice accretion tests were performed in a climatic chamber (Memmert CTC-256) at constant temperatures of −1, −2, −3, and −5 °C and relative humidity of 56% ± 3%. After thermal equilibrium, very small supercooled water droplets at −1 °C were sprayed onto the substrates with a speed of 0.05 mL/s for 10 min (a total of 30 mL of supercooled water) through a spray gun using constant pressure compressed air. The rate of the compressed air was kept constant at 17 m³/h by using a flowmeter. The distance between the spray gun and the substrate was 18 cm. Relative humidity of the

climatic chamber was increased from about 56% to 83% RH (±3% RH) during the spray process. The change of relative humidity of the climatic chamber with the change of sprayed supercooled water is given in Figure S1. After the spray, the samples were rapidly removed from the chamber, and the mass gain due to the ice accretion on the surface was gravimetrically determined in less than 15 s. Representative photographs of the spray gun ice accretion test system are shown in Figure S2. Supercooled water at −1 °C was sucked by the spray gun through a polyurethane hose from a graduated cylinder. The temperature of the supercooled water in the graduated cylinder was controlled precisely by heat transfer from an external Lauda circulator (for example, circulating liquid temperature was set to 1.2 °C for the experiments to be carried out at −2 °C in the chamber). The variables of the spray gun were kept constant for all of the experiments. Spraying started with the introduction of the compressed air via a manually controlled valve and ended after 10 min with the same valve. Because there are small differences in the sprayed water quantities in independent experiments within ±10%, then a calibration curve was prepared to normalize all of the mass increase values of experiments to a constant 30 mL water spray quantity, and these values are reported in the text. All of the samples were weighed before and after the test to calculate the mass increase, their surface areas were also previously determined, and ice accretion results are reported in (g/m²) units.

Drop Freezing Time. Drop freezing time is the time needed for the water drops present on a surface to freeze in a subzero temperature medium. Temperature and relative humidity of the Memmert CTC-256 climatic chamber were kept constant at −10 °C and 58 ± 3% RH, respectively, during the drop freezing time measurements. After equilibrium in the chamber, water droplets having 24 μL volume were injected onto test surfaces by a motorized syringe, which was located outside the chamber through a very small hole on the wall of the chamber. Representative photographs of the test system are given in Figure S3. Tap water is used instead of ultrapure water in these experiments to prevent the unexpectedly rapid freezing of the droplets due to instability of the supercooled pure water. Initially, the water drops were all transparent on the surfaces and became translucent/white after being frozen by time. Drop freezing times were recorded when a droplet becomes translucent and reported as the average of 10 measurements.

Ice Adhesion Test. 50 μL water droplets were placed on the test surface by a syringe at room conditions, and the samples were rapidly moved to a laboratory deep freezer at −30 °C and kept there for 15 min. After freezing of the drop, the sample was moved to a Memmert CTC-256 climatic chamber where a tensiometer and micrometric controlled 2D placer was previously located and cooled. The

temperature and relative humidity of the climatic chamber were kept constant at −10 °C and 58% ± 3% RH, respectively, during the ice adhesion measurements. After the sample was kept in the climatic chamber for 15 min, the force required to detach each frozen water drop on the samples was measured by propelling the probe of an analogue force transducer Geratech SN-20/50 (or Sundoo SN-10 in some experiments) horizontally into the side of a frozen water drop at a constant velocity of roughly 0.25 mm/s using a manually controlled 2D placer where the speed of movement is adjusted through a hole in the wall of the climatic chamber. The probe was located less than 1 mm above the substrate surface to minimize torque on the ice. The value of applied maximum force at the break moment of the ice drop was recorded. The diameters of the frozen droplets were varied according to the substrate type and measured precisely in parallel experiments. The representative photographs of the test system are given in Figure S4. Because water spreads on liquid swollen filter paper, no direct experimental ice adhesion strength measurement can be done. However, an indirect method was also applied to these surfaces: Frozen droplets having 50 μL volumes were formed in the deep freezer at −30 °C and then placed onto the hydrophilic liquid swollen filter paper in the climatic chamber and kept here for 15 min to maintain ice adhesion with the substrate. The same dynamometer force test then was applied again. In all cases, shear strength of ice adhesion, which represents the resistance to shear separation at the ice−substrate interface, was calculated as

$$P = \frac{40F}{\pi d^2} \tag{1}$$

where P is ice adhesion strength (kPa), F is the maximum force at break recorded by the analogue force gauge meter (N), and d is the diameter of the ice droplet (cm).

Contact Angle Measurements. Static equilibrium water contact angles under air (θ_e) were measured by using a KSV-CAM 200 contact angle meter with a PC controlled motorized syringe within 0.5° precision after removing the needle from the drop as the average values of five measurements. Water is of spectroscopic grade and droplets with a volume of 5 μL were formed on substrates for equilibrium contact angles, and only the initial values, which were recorded 2 s after the release of the needle, were reported as the equilibrium contact angle. Advancing (θ_a) and receding (θ_r) water contact angles were also measured on the sample surfaces by increasing the volume of the droplets through a needle from 3 to 8 μL and decreasing from 8 to 3 μL, respectively, by using the automatic dispenser while the needle was kept within the liquid droplet.

Evaporation of Solvents from FP Support at Room Temperature. Mass loss of the EG, FA, GLY-85%, PAO, SiO, and Fluorinert FC-70 solvents from the FP surface was determined gravimetrically for 15 consecutive days in an open area under laboratory conditions.

■ RESULTS AND DISCUSSION

Surface Properties of Reference Metal and Polymer Substrates. Static equilibrium (θ_e), advancing (θ_a) and receding (θ_r) contact angles of water droplets, and contact angle hysteresis (CAH = $\theta_a - \theta_r$) values are shown in Table 1. Repeatable θ_e and θ_a results within ±1° were obtained on reference metal and plastic substrate surfaces, which can be assumed to be practically flat. It was determined that all of the metal and polymer reference materials were hydrophobic (or nearly hydrophobic) having a θ_a value of 82−110°. CAH values of metals (Cu and Al) were nearly twice those of polymers (PP and PTFE) showing their high surface roughness and also strong water/metal interaction, causing pinning of the three-phase contact line of the droplet.

Surface Properties of Solid Supports and Solvent Impregnated Surfaces. θ_e, θ_a, θ_r, and CAH values of water droplets on solid supports and solvent impregnated surfaces are

Table 1. Static Equilibrium (θ_e), Advancing (θ_a) and Receding (θ_r) Contact Angles, Contact Angle Hysteresis (CAH), and Drop Freezing Time Results of Water Drops for Copper, Aluminum, and PTFE and Various Solvent Impregnated Surfaces[a]

substrate	θ_e (±1°)	θ_a (±1°)	θ_r (±2°)	CAH (±3°)	drop freezing time (s)
copper	75	82	23	59	40 ± 7
aluminum	88	91	38	53	64 ± 10
PP	95	95	71	24	148 ± 10
PTFE	105	110	78	32	315 ± 30
PP-sorbent sheet	135	146	124	22	70 ± 5
SiO impregnated PP-sorbent sheet	95	104	85	19	47 ± 4
PAO impregnated PP-sorbent sheet	97	102	78	24	56 ± 4
Siloxane D5 impregnated PP-sorbent sheet	103	108	72	36	73 ± 7
filter paper (FP)		spreading			
SiO, PAO, Siloxane D5, EG, FA, GLY-85%, and Fluorinert FC-70 impregnated FP surfaces		spreading			

[a]SiO, silicone oil 350 cSt; PAO, polyalphaolefin; EG, ethylene glycol; FA, formamide; GLY-85%, water (15%)−glycerine (85% by wt) mixture.

given in Table 1. θ_e and θ_a results of the PP-sorbent sheet (135°, 146°) were much larger than those of the flat PP layer (95°, 95°), indicating the presence of air pockets on this hydrophobic fiber mat surface. However, its CAH result (22°) was similar to that of the PP layer (24°), showing that there were not large surface protrusions of varying lengths on the blank mat surface to pin the three-phase contact line of the water droplet. On the other hand, water droplet spreads on hydrophilic cellulose-based filter paper (FP) as expected. Water droplets also spread on SiO, PAO, Siloxane D5, EG, FA, GLY-85%, and Fluorinert FC-70 impregnated FP surfaces. Meanwhile, θ_a results of SiO, PAO, and Siloxane D5 impregnated PP-sorbent sheet samples were 104°, 102°, and 108°, respectively, indicating that these hydrophobic solvents form a continuous layer on the PP-sorbent sheet and their weak interaction with the water droplet resulted in the high contact angles. However, these contact angles are considerably smaller than the θ_a results of blank PP-sorbent sheet (146°) showing that the air pockets were removed from the sorbent surface during the solvent impregnation process. The spreading of water droplets on SiO, PAO, and Siloxane D5 impregnated FP surfaces indicates the presence of cellulose fibers on the top of the surface after the impregnation process, and no continuous layer of hydrophobic solvent was present on the surface. To check the solvent quantity after impregnation that would affect the final surface structure, we determined the liquid mass over support mass ratio at room temperature after equilibrium, and the results are given in Table 2. Hydrophobic PP-sorbent sheet support could carry 5.96−8.16 times hydrophobic solvents over its own weight, but hydrophilic FP could only carry 1.63−2.06 times hydrophobic solvents as seen in Table 2. These results explain why water droplets spread on SiO, PAO, and Siloxane D5 impregnated FP surfaces. The same behavior was also valid for the hydrophobic PP-sorbent sheet so that it could only carry 1.09−1.47 times hydrophilic solvents over its own weight and the hydrophilic FP could carry 2.71−2.80 times hydrophilic

Table 2. Impregnated Liquid Mass over Support Mass Ratio at Room Temperature and Ice Accretion Test Results for Metal, Plastic, and Various Solvent Impregnated Surfaces at −2 °C

substrate	impregnated liquid	impregnated liquid mass over support mass ratio	ice accretion (g/m^2)
copper			1006 ± 49
aluminum			880 ± 30
PTFE			742 ± 33
PP			933 ± 42
PP-sorbent sheet			885 ± 26
filter paper			845 ± 41
PP-sorbent sheet	water	1.09	880 ± 12
PP-sorbent sheet	PAO	5.96	895 ± 18
PP-sorbent sheet	SiO	8.16	841 ± 15
PP-sorbent sheet	Siloxane D5	7.77	839 ± 17
PP-sorbent sheet	EG	1.28	723 ± 54
PP-sorbent sheet	FA	1.12	677 ± 16
PP-sorbent sheet	GLY-85%	1.47	515 ± 58
filter paper	water	2.79	815 ± 20
filter paper	PAO	1.68	908 ± 14
filter paper	SiO	1.63	901 ± 15
filter paper	Siloxane D5	2.06	811 ± 9
filter paper	EG	2.72	509 ± 18
filter paper	Fluorinert FC-70	2.71	498 ± 17
filter paper	FA	2.73	464 ± 31
filter paper	GLY-85%	2.80	266 ± 14

solvents. These findings indicate that hydrophobic lubricants should be used with hydrophobic supports, and hydrophilic lubricants should be used with hydrophilic supports.

On the other hand, the fiber diameters of blank PP-sorbent sheet (4−10 μm) are 3−4 times smaller than those of the fibers of FP (10−30) μm as seen in the SEM images given in Figure 1, and this is another reason why PP-sorbent sheet could carry so much impregnated solvent while FP allows the drainage of a considerable part of the impregnated solvents to reach equilibrium. In summary, the texture of the solid support is an important parameter for the investigation of the liquid impregnated anti-icing surfaces, both in the extent of solid/liquid interaction (interfacial area) and also in the prevention of lubricant evaporation and drainage, which leaves the top surface uncoated by the lubricant.

Ice Accretion Results on Reference Substrates and Solvent Impregnated Surfaces. Ice accretion (or ice accumulation) on surfaces is the most important property to evaluate the anti-icing properties of a surface because the objective of any anti-icing research is to stop or decrease the ice formation on a surface. The main reason for icing in nature is the direct contact and adhesion of supercooled water droplets onto a solid surface in subzero temperature conditions, and any anti-icing test must consider that point. However, supercooled water spray test methods were not used in most of the published anti-icing literature probably due to the difficulty and high cost of simulating the natural icing conditions.[9] It is well-known that supercooling is a process where a liquid (or gas)

cools below its freezing point without solidification and supercooled droplets freeze immediately when contacted with a surface while ice nucleation begins. As given in the Experimental Section, we developed an ice accretion test system using sprayed supercooled water droplets onto samples. It is very difficult (if not impossible) to obtain an ice free surface in such a test system at subzero temperatures; however, it is possible to distinguish the differences of the mass of accreted ice on test surfaces, which would help in choosing the better anti-icing surface.

Ice accretion test results in mass per unit area units for metal, plastic, and various solvent impregnated surfaces at −2 °C are given in Table 2. Ice accretion on the reference solid surfaces decreased in the following order: Cu (1006 ± 49) > PP (933 ± 42) > Al (880 ± 30) > PTFE (742 ± 33 g/m^2). Blank PP-sorbent sheet (885 ± 26) and FP (845 ± 41 g/m^2) ice accretion results were also determined to be in this range. When the hydrophobic PP-sorbent sheet was used, the impregnation of the hydrophobic solvents did not help to improve the ice accretion properties of the test surfaces, and the results varied between 839 ± 17 and 895 ± 18 g/m^2. However, the impregnation of hydrophilic solvents onto hydrophobic PP-sorbent sheet decreased the ice accretion in the following order: EG (723 ± 54) > FA (677 ± 16) > GLY-85% (515 ± 58 g/m^2). The test result of water impregnated PP-sorbent surface (880 ± 12 g/m^2) was also high and similar to that of blank PP-sorbent sheet (885 ± 26 g/m^2), indicating that water cannot form a continuous layer on the hydrophobic PP-sorbent mat surface. The impregnation results of hydrophilic solvents onto hydrophobic PP-sorbent sheet can be considered as "good" because the ice accretion results are less than all of the metal and polymer reference surfaces.

On the other hand, when hydrophilic support FP is used, then the impregnation of hydrophobic solvents did not help to improve the ice accretion properties, and the test results varied between 811 ± 9 and 908 ± 14 g/m^2. However, the impregnation of hydrophilic solvents onto hydrophilic FP support decreased the ice accretion considerably in the following order: EG (509 ± 18) > FA (464 ± 31) > GLY-85% (266 ± 14 g/m^2). Water impregnation on FP (815 ± 20 g/m^2) resulted in a value similar to that of blank FP (845 ± 41 g/m^2), indicating that water cannot form a continuous layer on hydrophilic FP layer surface and freezes easily in the cold test chamber to accumulate more ice. We also tested the fluorinated lubricant (Fluorinert FC-70), which was used in the publications of Aizenberg and co-workers in our ice accretion system and determined a value of 498 ± 17 g/m^2 that is also good, but much larger than the result of the GLY-85% impregnated FP surface (266 ± 14 g/m^2). Ice accretion results on different solvent impregnated FP surfaces at −2 °C are given in Figure 2. No significant decrease of ice accretion was observed on the hydrophobic PAO, SiO, and Siloxane D5 impregnated FP surfaces in comparison with the metal and polymer reference surfaces. On the other hand, the ice accretion results for the EG, FA, and GLY-85% impregnated surfaces on FP were much lower than those of hydrophobic solvent impregnated surfaces.

The freezing of a supercooled droplet is a two-stage process. Nucleation starts in the first stage, and the nucleus grows afterward. Heterogeneous nucleation occurs at a surface, and the inhibition of the nucleation is the most important point.[9] All of the used hydrophilic solvents in impregnation of FP and PP-sorbent have hydrogen-bonding ability with water due to
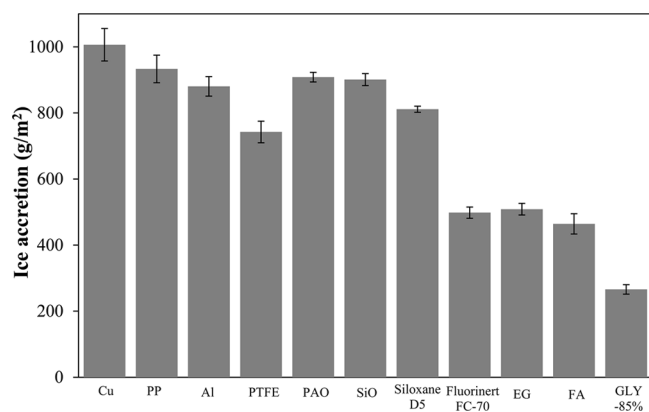
Figure 2. Ice accretion values (g/m^2) on solvent impregnated filter paper surfaces at -2 °C.

the presence of hydroxyl $(-OH)$ or amide $(-NH)$ groups in their structure. Thus, the high reduction of ice accretion on GLY-85% impregnated FP can be attributed to three parameters: (1) the formation of hydrogen bonds with impacting supercooled water and the hydroxyl groups of GLY-85%; (2) the corresponding freezing point depression to prevent the instantaneous freezing of a supercooled droplet; and (3) the high mobility of the hydroxyl groups in GLY-85% allowing hydrogen-bonding ease with impacting water droplets. This mechanism is completely different from that of SLIPS icephobicity where contact angle hysteresis and contact line pinning properties were minimized to impart icephobicity.[43,45]

We also reported the ice accretion results, which were performed at -2 °C of solvent impregnated PP-sorbent sheet and FP in Figure 3 to compare the effect of the nature of the
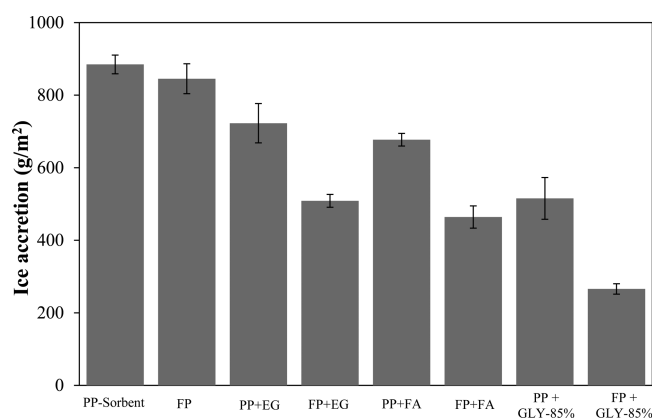

Figure 3. Comparison of ice accretion values (g/m^2) of solvent impregnated PP-sorbent sheet and filter paper surfaces. Ice accretion tests were performed at -2 °C. EG, ethylene glycol; FA, formamide; GLY-85%, water (15%)−glycerine (85% by wt) mixture.

solid support. It is clearly seen in this figure that the use of a hydrophilic solid support after impregnation with a hydrophilic hydrogen-bonding solvent is more effective to decrease the ice accretion values on surfaces.

Effect of Temperature on the Ice Accretion Results. We also investigated ice accretion on Al, PTFE, and PP reference surfaces and solvent impregnated FP surfaces by decreasing the temperature in the climatic chamber ranging between -1 and -5 °C. Ice accretion results with varying temperatures on these surfaces are given in Table S1 and

plotted in Figure 4. It is seen that the ice accretion on both hydrophilic liquid impregnated FP surfaces and reference
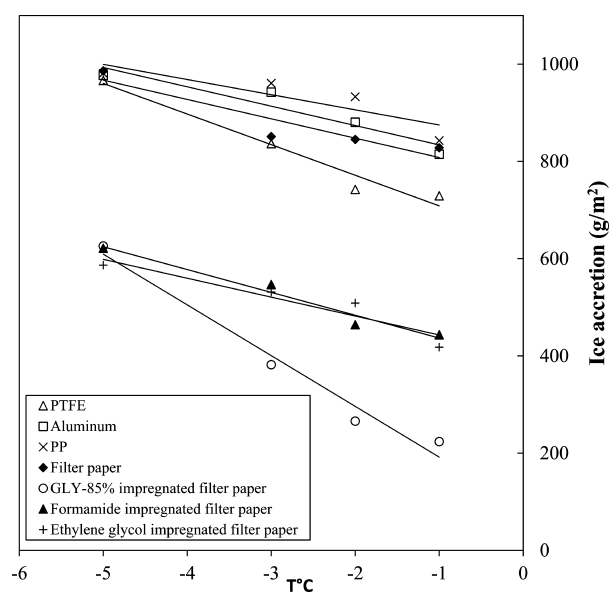
Figure 4. Change of ice accretion (g/m^2) with the change of air temperature of the climatic chamber while spraying of supercooled water onto surfaces. Initial relative humidity of the test medium was 56% $\pm$ 3% RH.

surfaces increased almost linearly with the decrease of the temperature in the climatic chamber. Ice accretion results on the EG, FA, and GLY-85% impregnated surfaces were found to be very close to each other at -5 °C around 600 g/m^2 and on reference surfaces around 970 g/m^2. It is possible that the freezing point depression property of hydrogen-bonding liquids, which were impregnated on the surface to impacting supercooled water droplets, is not so effective when the temperature of the medium cools. These findings were also supported by other published reports. For example, Yang et al.[40] reported that ice accretion values on PTFE and Al reference surfaces were very close to each other at -8 °C. It is determined that, although the efficiency decreased, hydrophilic liquid impregnation on surfaces is still advantageous at -5 °C when the results of reference and solvent impregnated surfaces are compared.

Snow Accretion Test Results. We also tested natural snow accretion on PTFE, Al reference surfaces, and hydrophilic solvent impregnated filter paper surfaces in a heavy snowfall in 12 January 2015 afternoon in Gebze, Turkey, where the temperature during the snowfall was measured to be 0 °C, RH = 60% $\pm$ 5%, wind velocity = 53 km/h. The sample surfaces were placed with an angle of 30° to the horizontal during this test. Snow accretion results are given in Table 3. As seen in this table, the order of the snow accretion results of all of the tested surfaces is the same with the ice accretion results obtained in the climatic chamber in the laboratory, which were given in Table 2, although natural snow accretion results were approximately twice the ice accretion results. It is possible that large interconnected snow particles can be accumulated on surfaces more rapidly at subzero temperatures than the supercooled water microdroplets spraying from the nozzle.

Solvent Evaporation from the Impregnated FP Surface Results. We also investigated how long the impregnated hydrophilic and fluorinated solvents can stay inside the solid FP

Table 3. Snow Accretion Test Results for Aluminum, PTFE, and Various Solvent Impregnated Filter Paper Surfaces in Snowfall at 0 °C, RH = 60% ± 5%, Wind Velocity = 53 km/h in 12 January 2015 Afternoon in Gebze, Turkey, Where the Angle between Sample Surface and Floor Was 30°

substrate	impregnated liquid	impregnated liquid mass over support mass ratio	snow accretion (g/m^2)
aluminum			1465
PTFE			1407
filter paper	EG	2.72	1054
filter paper	FA	2.73	943
filter paper	GLY-85%	2.80	686

support before evaporating completely. Normalized mass loss of the EG, FA, GLY-85%, PAO, SiO, and Fluorinert FC-70 solvents from the FP surface, which was determined gravimetrically for 15 consecutive days in an open area under laboratory conditions, is given in Figure 5. Fluorinert FC-70
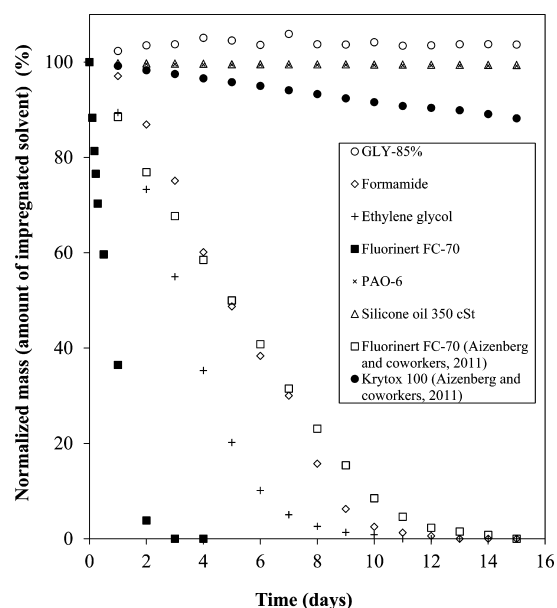
Figure 5. Evaporation behaviors of different solvents from filter paper surface at room temperature.

was evaporated completely before 3 days and EG and FA before 10 days. Hydrophobic PAO, SiO, and hydrophilic GLY-85% stayed inside the FP without evaporating over 15 days. This is due to the very low vapor pressures of these liquids. We also determined that there is an increase in the total mass of GLY-85% impregnated surface due to water vapor adsorption from the surrounding because it is hygroscopic. In summary, the evaporation problems of GLY-85%, SiO, and PAO impregnated FP surfaces were minimal, and these lubricating liquids can remain a considerably long time on the supporting solid surface.

Effect of Synthetic Rain and Repeated Ice Accretion Tests on the Durability of Glycerine−Water Impregnated Filter Paper Support. We investigated the durability of glycerine−water impregnated filter paper surfaces against synthetic rain and also repeated ice accretion tests and determined that the GLY-85% impregnated FP sample lost its ice-phobicity slowly with the decrease of the GLY-85% mass on the textured FP support. We sprayed cold water onto

sample surfaces in cold medium to simulate rain effect. It was determined that around 20% mass of the impregnated GLY-85% on the filter paper was removed from the surface after we sprayed five times with 5 mL of water at 10 °C, onto GLY-85% impregnated FP, which was kept at 10 °C in the cooling chamber. The composition of the glycerine/water mixture was also changed with the increase of the water content during this test. The mass of accreted ice of this surface increased from 266 to 546 g/m^2 when the ice accretion test was applied at −2 °C, indicating that the population of the cellulosic protrusions of the textured surface on the top of the sample surface increased by washing with the rain spray and the ice nucleation increased with the loss of the lubricating fluid. In addition, we repeated ice accretion experiments at −2 °C one after another using the same GLY-85% impregnated filter paper sample and found that it lost its ice-phobicity after two or three tests. In conclusion, a continuous supply of the hydrophilic lubricating liquid from a liquid reservoir onto textured ice-phobic surfaces would become necessary to maintain the replenishment of the hydrophilic liquid for the sustained performance.[54]

Drop Freezing Delay Results. The freezing periods of water drops on the solid reference surfaces were found to increase in the following order with the increase of the equilibrium contact angle of the surfaces from 75° to 105°: Cu (40 ± 7 s) < Al (64 ± 10 s) < PP (148 ± 10 s) < PTFE (315 ± 30 s), as given in Table 1. PTFE was found to have the longest drop freezing time, indicating that the fluorine-containing PTFE surface is more effective for delaying the ice nucleation possibly due to its low surface free energy. Drop freezing times of the hydrophobic liquid impregnated PP-sorbent sheet surfaces increased in the following order: SiO (47 ± 4 s) < PAO (56 ± 4 s) < blank PP-sorbent mat (70 ± 5 s) < Siloxane D5 (73 ± 7 s), as given in the same table. It was determined that the use of hydrophobic solvent impregnation did not impart drop freezing delay. On the other hand, no drop freezing period can be determined on blank FP and solvent impregnated FP surfaces because of the initial spreading of water droplets on these surfaces, and a comparison cannot be made on the drop freezing delay results of them with the reference substrates.

Ice Adhesion Strength Results. Ice adhesion strength results of water drops on the solid reference surfaces were found to decrease in the following order: Cu (1217 ± 34) > Al (731 ± 53) > PP (640 ± 36) > PTFE (268 ± 13 kPa), as given in Table 4. These results are comparable to some of the literature reports: Menini et al.[21] reported 505 kPa, Dou et al.[57]

Table 4. Ice Adhesion Strength Test Results for Reference Metal, Plastic, and Solvent Impregnated Surfaces[a]

substrate	ice adhesion strength (kPa)
copper	1217 ± 34
aluminum	731 ± 53
PTFE	268 ± 13
PP	640 ± 36
PAO impregnated filter paper	138 ± 32
SiO impregnated filter paper	133 ± 9
Siloxane D5 impregnated filter paper	113 ± 24
EG, FA, GLY-85%, and Fluorinert FC-70 impregnated filter paper	16 ± 3

[a]PAO, polyalphaolefin; EG, ethylene glycol; FA, formamide; GLY-85%, water (15%)−glycerine (85% by wt) mixture.

reported 800 kPa, and we measured 731 kPa for ice adhesion strength of Al; and 1020 kPa was found for Cu,[57] while we measured 1217 kPa. Similarly, Menini et al.[21] reported 209 kPa for ice adhesion strength of PTFE surface, which is a very close value to our PTFE result (268 kPa), indicating that our experimental setup for ice adhesion strength measurements gives reasonable data. There is an inverse relationship between the water contact angle and ice adhesion strength of a surface similar to the literature reports,[21,38,41] and ice adhesion of the solid reference surfaces decreased from 1217 to 268 kPa with the increase of the contact angle of the substrates from 75° to 105° in our work. On the other hand, ice adhesion strengths on the GLY-85%, FA, and EG impregnated FP surfaces are very low and nearly constant at 16 ± 3 kPa. Similarly, Kim et al.[44] reported the ice adhesion strength of perfluorinated lubricant (Krytox-100) impregnated polypyrrole-coated Al to be 15.6 ± 3.6 kPa, and Dou et al.[57] reported 27.0 ± 6.2 kPa for dimethylolpropionic acid impregnated polyurethane surface, which are both very close to our results. Chen et al.[55] reported the ice adhesion strength of water impregnated hygroscopic poly(acrylic acid) surfaces to be 55 ± 15 kPa, which is more than 3 times larger than our results. It is determined that the ice droplets can be easily removed from the liquid impregnated surfaces after ice formation by the application of a quite very low shear force because these liquid-coated surfaces can only make a very weak adhesion with ice. The impregnated lubricant between the substrate surface and the formed ice weakens the interaction between the ice and the solid. Consequently, hydrophilic solvent impregnated FP surfaces were also found to be advantageous when an anti-icing coating was aplied to decrease the ice adhesion strength considerably.

CONCLUSIONS

In this work, hydrophobic liquids such as fluorinated aliphatics, polyalphaolefin, decamethylcyclopenta siloxane, and silicone oil, and also hydrophilic liquids such as ethylene glycol, formamide, water, and water−glycerine mixture were impregnated onto a hydrophobic polypropylene sorbent mat and hydrophilic cellulose-based filter paper surfaces. Ice accretion, drop freezing time, and ice adhesion strength properties of these test surfaces then were examined, and the results were compared to reference surfaces such as aluminum, copper, polypropylene, and polytetrafluoroethylene. An ice accretion test method was also developed to investigate the increase of the mass of formed ice gravimetrically by spraying supercooled water onto these surfaces at different subzero temperatures ranging between −1 and −5 °C.

It was determined that hydrophilic solvent (especially water−glycerine 15:85% by wt mixture) impregnated hydrophilic porous surfaces would be a promising candidate for anti-icing applications because these surfaces decrease both the ice accretion and the ice adhesion strength properties especially at −2 °C temperature. The interaction between the substrate and ice was very low for hydrophilic solvent impregnated surfaces, giving very low ice adhesion strength (16 ± 3 kPa). The high reduction of ice accretion on the GLY-85% impregnated FP sample was attributed to the formation of hydrogen bonds with impacting supercooled water droplet and the hydroxyl groups of glycerine solution layer on the surface and the corresponding freezing point depression to prevent the instantaneous freezing of the supercooled droplet. The mass of accreted ice on the surfaces increased with the decrease of the temperature of the test medium down to −5 °C, getting closer to each other but

still advantageous when compared to the reference metal and polymer surfaces. The removal of water-soluble hydrophilic lubricants from the support by rain or snow is a problem, and a continuous supply of the hydrophilic lubricant from a liquid reservoir onto the textured support would become necessary to maintain the replenishment of the lubricant for the sustained performance. Other water/glycerine or similar hydrophilic compositions having low freezing points impregnated by other suitable hydrophilic supporting solids can be promising coatings with good icephobic properties.

ASSOCIATED CONTENT

Supporting Information

The Supporting Information is available free of charge on the ACS Publications website at DOI: 10.1021/acsami.5b07265.

Table giving ice accretion test results for PTFE, aluminum, PP, and various solvent impregnated surfaces; a graphic including change of relative humidity of the climatic chamber with the volume change of the sprayed supercooled water; photographs of the ice accretion test system using the Memmert CTC 256 climatic chamber; photograph of the motorized syringe, which is used to form droplets inside the climatic chamber during drop freezing time experiments; and photograph of ice adhesion test system in the climatic chamber using a tensiometer and 2D placer (PDF)

AUTHOR INFORMATION

Corresponding Author

*Phone: +90 262 605 2114. E-mail: yerbil@gtu.edu.tr.

Notes

The authors declare no competing financial interest.

REFERENCES

(1) Marwitz, J.; Politovich, M.; Bernstein, B.; Ralph, F.; Neiman, P.; Ashenden, R.; Bresch, J. Meteorological Conditions Associated with The ATR72 Aircraft Accident Near Roselawn, Indiana, on 31 October 1994. *Bull. Am. Meteorol. Soc.* **1997**, *78*, 41−52.

(2) Makkonen, L.; Laakso, T.; Marjaniemi, M.; Finstad, K. J. Modeling and Prevention of Ice Accretion on Wind Turbines. *Wind Eng.* **2001**, *25*, 3−21.

(3) Dalili, N.; Edrisy, A.; Carriveau, R. A Review of Surface Engineering Issues Critical to Wind Turbine Performance. *Renewable Sustainable Energy Rev.* **2009**, *13*, 428−38.

(4) Parent, O.; Ilinca, A. Anti-Icing and De-Icing Techniques for Wind Turbines: Critical Review. *Cold Reg. Sci. Technol.* **2011**, *65*, 88−96.

(5) Laforte, J. L.; Allaire, M. A.; Laflamme, J. State-of-the-art on Power Line De-Icing. *Atmos. Res.* **1998**, *46*, 143−158.

(6) Ryerson, C. C. Ice Protection of Offshore Platforms. *Cold Reg. Sci. Technol.* **2011**, *65*, 97−110.

(7) Fillion, R. M.; Riahi, A. R.; Edrisy, A. A Review of Icing Prevention in Photovoltaic Devices by Surface Engineering. *Renewable Sustainable Energy Rev.* **2014**, *32*, 797−809.

(8) Meuler, A. J.; McKinley, G. H.; Cohen, R. E. Exploiting Topographical Texture to Impart Icephobicity. *ACS Nano* **2010**, *4*, 7048−7052.

(9) Lv, J.; Song, Y.; Jiang, L.; Wang, J. Bio-Inspired Strategies for Anti-Icing. *ACS Nano* **2014**, *8*, 3152−3169.

(10) Schutzius, T. M.; Jung, S.; Maitra, T.; Eberle, P.; Antonini, C.; Stamatopoulos, C.; Poulikakos, D. Physics of Icing and Rational Design of Surfaces with Extraordinary Icephobicity. *Langmuir* **2015**, *31*, 4807−4821.

(11) Muthumani, A.; Fay, L.; Akin, M.; Wang, S.; Gong, J.; Shi, X. Correlating Lab and Field Tests for Evaluation of Deicing and Anti-Icing Chemicals: A Review of Potential Approaches. *Cold Reg. Sci. Technol.* **2014**, *97*, 21−32.

(12) Darmanin, T.; Guittard, F. Recent Advances in the Potential Applications of Bioinspired Superhydrophobic Materials. *J. Mater. Chem. A* **2014**, *2*, 16319−16359.

(13) Erbil, H. Y.; Demirel, A. L.; Avci, Y.; Mert, O. Transformation of a Simple Plastic into a Superhydrophobic Surface. *Science* **2003**, *299*, 1377−1380.

(14) Ozbay, S.; Erbil, H. Y. Superhydrophobic and Oleophobic Surfaces Obtained by Graft Copolymerization of Perfluoroalkyl Ethyl Acrylate onto SBR Rubber. *Colloids Surf., A* **2015**, *481*, 537−546.

(15) Cao, L.; Jones, A. K.; Sikka, V. K.; Wu, J.; Gao, D. Anti-Icing Superhydrophobic Coatings. *Langmuir* **2009**, *25*, 12444−12448.

(16) Kulinich, S. A.; Farzaneh, M. Ice Adhesion on Super-hydrophobic Surfaces. *Appl. Surf. Sci.* **2009**, *255*, 8153−8157.

(17) Kulinich, S. A.; Farzaneh, M. How Wetting Hysteresis Influences Ice Adhesion Strength on Superhydrophobic Surfaces. *Langmuir* **2009**, *25*, 8854−8856.

(18) Wang, F.; Li, C.; Lv, Y.; Lv, F.; Du, Y. Ice Accretion on Superhydrophobic Aluminum Surfaces under Low-Temperature Conditions. *Cold Reg. Sci. Technol.* **2010**, *62*, 29−33.

(19) Antonini, C.; Innocenti, M.; Horn, T.; Marengo, M.; Amirfazli, A. Understanding the Effect of Superhydrophobic Coatings on Energy Reduction in Anti-icing Systems. *Cold Reg. Sci. Technol.* **2011**, *67*, 58−67.

(20) He, M.; Wang, J.; Li, H.; Song, Y. Superhydrophobic Surfaces to Condensed Micro-droplets at Temperatures below the Freezing Point Retard Ice/Frost Formation. *Soft Matter* **2011**, *7*, 3993−4000.

(21) Menini, R.; Ghalmi, Z.; Farzaneh, M. Highly Resistant Icephobic Coatings on Aluminum Alloys. *Cold Reg. Sci. Technol.* **2011**, *65*, 65−69.

(22) Guo, P.; Zheng, Y.; Wen, M.; Song, C.; Lin, Y.; Jiang, L. Icephobic/Anti-Icing Properties of Micro/Nanostructured Surfaces. *Adv. Mater.* **2012**, *24*, 2642−2648.

(23) Ruan, M.; Li, W.; Wang, B.; Deng, B.; Ma, F.; Yu, Z. Preparation and Anti-icing Behavior of Superhydrophobic Surfaces on Aluminum Alloy Substrates. *Langmuir* **2013**, *29*, 8482−8491.

(24) Boinovich, L. B.; Emelyanenko, A. M. Anti-icing Potential of Superhydrophobic Coatings. *Mendeleev Commun.* **2013**, *23*, 3−10.

(25) Arianpour, F.; Farzaneh, M.; Kulinich, S. A. Hydrophobic and Ice-Retarding Properties of Doped Silicone Rubber Coatings. *Appl. Surf. Sci.* **2013**, *265*, 546−552.

(26) Bharathidasan, T.; Kumar, S. V.; Bobji, M. S.; Chakradhar, R. P. S.; Basu, B. J. Effect of Wettability and Surface Roughness on Ice-adhesion Strength of Hydrophilic, Hydrophobic and Superhydrophobic Surfaces. *Appl. Surf. Sci.* **2014**, *314*, 241−250.

(27) Davis, A.; Yeong, Y. H.; Steele, A.; Bayer, I. S.; Loth, E. Superhydrophobic Nanocomposite Surface Topography and Ice Adhesion. *ACS Appl. Mater. Interfaces* **2014**, *6*, 9272−9279.

(28) Varanasi, K. K.; Deng, T.; Smith, J. D.; Hsu, M.; Bhate, N. Frost Formation and Ice Adhesion on Superhydrophobic Surfaces. *Appl. Phys. Lett.* **2010**, *97*, 234102.

(29) He, M.; Li, H.; Wang, J.; Song, Y. Superhydrophobic Surface at Low Surface Temperature. *Appl. Phys. Lett.* **2011**, *98*, 093118.

(30) Farhadi, S.; Farzaneh, M.; Kulinich, S. A. Anti-icing Performance of Superhydrophobic Surfaces. *Appl. Surf. Sci.* **2011**, *257*, 6264−6269.

(31) Jung, S.; Dorrestijn, M.; Raps, D.; Das, A.; Megaridis, C. M.; Poulikakos, D. Are Superhydrophobic Surfaces Best for Icephobicity? *Langmuir* **2011**, *27*, 3059−3066.

(32) Kulinich, S. A.; Farhadi, S.; Nose, K.; Du, X. W. Super-hydrophobic Surfaces: Are They Really Ice-Repellent? *Langmuir* **2011**, *27*, 25−29.

(33) Chen, J.; Liu, J.; He, M.; Li, K.; Cui, D.; Zhang, Q.; Zeng, X.; Zhang, Y.; Wang, J.; Song, Y. Superhydrophobic Surfaces Cannot Reduce Ice Adhesion. *Appl. Phys. Lett.* **2012**, *101*, 111603.

(34) Nosonovsky, M.; Hejazi, V. Why Superhydrophobic Surfaces are not Always Icephobic. *ACS Nano* **2012**, *6*, 8488−8491.

(35) Oberli, L.; Caruso, D.; Hall, C.; Fabretto, M.; Murphy, P. J.; Evans, D. Condensation and freezing of droplets on superhydrophobic surfaces. *Adv. Colloid Interface Sci.* **2014**, *210*, 47−57.

(36) Wang, H.; He, G.; Tian, Q. Effects of Nano-Fluorocarbon Coating on Icing. *Appl. Surf. Sci.* **2012**, *258*, 7219−7224.

(37) Saito, H.; Takai, K.; Yamauchi, G. Water and Ice-Repellent Coatings. *Surf. Coat. Int.* **1997**, *80*, 168−171.

(38) Meuler, A. J.; Smith, J. D.; Varanasi, K. K.; Mabry, J. M.; McKinley, G. H.; Cohen, R. E. Relationships between Water Wettability and Ice Adhesion. *ACS Appl. Mater. Interfaces* **2010**, *2*, 3100−3110.

(39) Yin, L.; Xia, Q.; Xue, J.; Yang, S.; Wang, Q.; Chen, Q. In situ Investigation of Ice Formation on Surfaces with Representative Wettability. *Appl. Surf. Sci.* **2010**, *256*, 6764−6769.

(40) Yang, S.; Xia, Q.; Zhu, L.; Xue, J.; Wang, Q.; Chen, Q. Research on the Icephobic Properties of Fluoropolymer-based Materials. *Appl. Surf. Sci.* **2011**, *257*, 4956−4962.

(41) Zou, M.; Beckford, S.; Wei, R.; Ellis, C.; Hatton, G.; Miller, M. A. Effects of Surface Roughness and Energy on Ice Adhesion Strength. *Appl. Surf. Sci.* **2011**, *257*, 3786−3792.

(42) Li, K.; Xu, S.; Shi, W.; He, M.; Li, H.; Li, S.; Zhou, X.; Wang, J.; Song, Y. Investigating the Effects of Solid Surfaces on Ice Nucleation. *Langmuir* **2012**, *28*, 10749−10754.

(43) Wong, T. S.; Kang, S. H.; Tang, S. K. Y.; Smythe, E. J.; Hatton, B. D.; Grinthal, A.; Aizenberg, J. Bioinspired Self-Repairing Slippery Surfaces with Pressure-Stable Omniphobicity. *Nature* **2011**, *477*, 443−447.

(44) Kim, P.; Wong, T. S.; Alvarenga, J.; Kreder, M. J.; Adorno-Martinez, W. E.; Aizenberg, J. Liquid-Infused Nanostructured Surfaces with Extreme Anti-Ice and Anti-Frost Performance. *ACS Nano* **2012**, *6*, 6569−6577.

(45) Stone, H. A. Ice-Phobic Surfaces That Are Wet. *ACS Nano* **2012**, *6*, 6536−6540.

(46) Wilson, P. W.; Lu, W.; Xu, H.; Kim, P.; Kreder, M. J.; Alvarenga, J.; Aizenberg, J. Inhibition of Ice Nucleation by Slippery Liquid-Infused Porous Surfaces (SLIPS). *Phys. Chem. Chem. Phys.* **2013**, *15*, 581−585.

(47) Kim, P.; Kreder, M. J.; Alvarenga, J.; Aizenberg, J. Hierarchical or Not? Effect of the Length Scale and Hierarchy of the Surface Roughness on Omniphobicity of Lubricant-Infused Substrates. *Nano Lett.* **2013**, *13*, 1793−1799.

(48) Vogel, N.; Belisle, R. A.; Hatton, B.; Wong, T. S.; Aizenberg, J. Transparency and Damage Tolerance of Patternable Omniphobic Lubricated Surfaces Based on Inverse Colloidal Monolayers. *Nat. Commun.* **2013**, *4*, 2176−2185.

(49) Erbil, H. Y. *Surface Chemistry of Solid and Liquid Interfaces*; Blackwell Publishing: Oxford, 2006.

(50) Erbil, H. Y. The Debate on the Dependence of Apparent Contact Angles on Drop Contact Area or Three-Phase Contact Line: A Review. *Surf. Sci. Rep.* **2014**, *69*, 325−365.

(51) Anand, S.; Paxson, A. T.; Dhiman, R.; Smith, J. D.; Varanasi, K. K. Enhanced Condensation on Lubricant-Impregnated Nanotextured Surfaces. *ACS Nano* **2012**, *6*, 10122−10129.

(52) Smith, J. D.; Dhiman, R.; Anand, S.; Reza-Garduno, E.; Cohen, R. E.; McKinley, G. H.; Varanasi, K. K. Droplet Mobility on Lubricant-Impregnated Surfaces. *Soft Matter* **2013**, *9*, 1772−1780.

(53) Subramanyam, S. B.; Rykaczewski, K.; Varanasi, K. K. Ice Adhesion on Lubricant-Impregnated Textured Surfaces. *Langmuir* **2013**, *29*, 13414−13418.

(54) Rykaczewski, K.; Anand, S.; Subramanyam, S. B.; Varanasi, K. K. Mechanism of Frost Formation on Lubricant-Impregnated Surfaces. *Langmuir* **2013**, *29*, 5230−5238.

(55) Chen, J.; Dou, R.; Cui, D.; Zhang, Q.; Zhang, Y.; Xu, F.; Zhou, X.; Wang, J.; Song, Y.; Jiang, L. Robust Prototypical Anti-icing Coatings with a Self-lubricating Liquid Water Layer between Ice and Substrate. *ACS Appl. Mater. Interfaces* **2013**, *5*, 4026−4030.

(56) Liu, H.; Zhang, P.; Liu, M.; Wang, S.; Jiang, L. Organogel-based Thin Films for Self-Cleaning on Various Surfaces. *Adv. Mater.* **2013**, *25*, 4477−4481.

(57) Dou, R.; Chen, J.; Zhang, Y.; Wang, X.; Cui, D.; Song, Y.; Jiang, L.; Wang, J. Anti-icing Coating with an Aqueous Lubricating Layer. *ACS Appl. Mater. Interfaces* **2014**, *6*, 6998−7003.

(58) Chen, J.; Luo, Z.; Fan, Q.; Lv, J.; Wang, J. Anti-Ice Coating Inspired by Ice Skating. *Small* **2014**, *10*, 4693−4699.

(59) Chen, L.; Geissler, A.; Bonaccurso, E.; Zhang, K. Transparent Slippery Surfaces Made with Sustainable Porous Cellulose Lauroyl Ester Films. *ACS Appl. Mater. Interfaces* **2014**, *6*, 6969−6976.

(60) Zhu, L.; Xue, J.; Wang, Y.; Chen, Q.; Ding, J.; Wang, Q. Ice-phobic Coatings Based on Silicon-Oil-Infused Polydimethylsiloxane. *ACS Appl. Mater. Interfaces* **2013**, *5*, 4053−4062.

(61) Eifert, A.; Paulssen, D.; Varanakkottu, S. N.; Baier, T.; Hardt, S. Simple Fabrication of Robust Water-Repellent Surfaces with Low Contact-Angle Hysteresis Based on Impregnation. *Adv. Mater. Interfaces* **2014**, *1*, 1300138.

(62) Yin, X.; Zhang, Y.; Wang, D.; Liu, Z.; Liu, Y.; Pei, X.; Yu, B.; Zhou, F. Integration of Self-Lubrication and Near-Infrared Photo-thermogenesis for Excellent Anti-Icing/Deicing Performance. *Adv. Funct. Mater.* **2015**, *25*, 4237−4245.

(63) Liu, Q.; Yang, Y.; Huang, M.; Zhou, Y.; Liu, Y.; Liang, X. Durability of a lubricant-infused Electrospray Silicon Rubber surface as an anti-icing coating. *Appl. Surf. Sci.* **2015**, *346*, 68−76.

(64) Wang, Y.; Yao, X.; Chen, J.; He, Z.; Liu, J.; Li, Q.; Wang, J.; Jiang, L. Organogel as Durable Anti-Icing Coatings. *Sci. China Mater.* **2015**, *58*, 559.

(65) Urata, C.; Dunderdale, G. J.; England, M. W.; Hozumi, A. Self-Lubricating Organogels (SLUGs) with Exceptional Syneresis-Induced Anti-Sticking Properties Against Viscous Emulsions and Ices. *J. Mater. Chem. A* **2015**, *3*, 12626−12630.